Adaptive Path Following for Unmanned Aerial Vehicles in Time-Varying Unknown Wind Environments*

Bingyu Zhou[1], Harish Satyavada[2] and Simone Baldi[1]

***Abstract*— In this paper, an adaptive control scheme for Unmanned Aerial Vehicles (UAVs) path following under slowly time-varying wind is developed. The proposed control strategy integrates the path following law based on the vector field method with an adaptive term counteracting the effect of wind's unknown component. In particular, it is shown that the path following error is bounded under slowly time-varying unknown wind and converges to zero for unknown constant wind. Numerical simulations illustrate that, in environments with unknown and slowly time-varying wind conditions, the proposed method compensates for the lack of knowledge of the wind vector, and attains a smaller path following error than state-of-the-art vector field method.**

I. INTRODUCTION

Unmanned aerial vehicles (UAVs) are versatile in many applications. Most tasks in the application fields, like the military surveillance at a certain target and the rescue task in the forest fire, rely on the accurate and robust path generator and path tracking controller in UAVs. The challenge of the path following controller design stems from the wind disturbance, UAV dynamic characteristics and the quality of the sensors. In this paper, the influence of wind on UAV behavior is the main consideration in the path following design procedure.

Several methods for UAV path following have been already proposed and tested on actual UAV platforms. In [1], state-of-the-art path following algorithms in 2D , such as the carrot-chasing algorithm, nonlinear guidance law (NLGL) [2], vector-field (VF)-based path following, LQR-based path following [3] [4] and pure pursuit with line-of-sight (PLOS)-based path following [5] are summarized and compared with each other using two metrics: total control effort and total cross-track error.

The basic concept of VF path following is to construct the vector field around the desired path to provide the course commands to the vehicle. Usually the path following laws are derived from Lyapunov stability analysis which guarantees the globally stable convergence to the desired path. The implementation of this concept is shown in [6], [7]. Another variation of Lyapunov vector field is proposed in [8], which is called tangent vector field guidance.

*This work has been partially sponsored by autoNomous, self-Learning, OPTImal and compLete Underwater Systems (NOPTILUS), Project Number: 270180, Funded by: EU FP7-ICT-2009.6. http://www.noptilus-fp7.eu/.

[1]Bingyu Zhou and Simone Baldi are with Delft Center for Systems and Control, 3ME, Delft University of Technology, 2628 CD, Delft, The Netherlands bryan-by@hotmail.com;S.Baldi@tudelft.nl

[2]Harish Satyavada is with GE Global Research (Wind Lab), Whitefield, Bangalore, India satyavada93@gmail.com

However, VF methods work under the assumptions of a perfectly known constant wind disturbance. The main contribution of this paper is to extend the standard vector field path following strategy [6] to the uncertain time-varying wind scenarios where the unknown and possibly time-varying wind components may add up to a constant wind component. In this work, the path following control law is augmented with an estimator counteracting the effects of the unknown wind component, thus resulting in an adaptive vector field path following strategy. Stability analysis is performed via Lyapunov methods which show the path following error is bounded under slowly time-varying unknown wind and converges to zero for unknown constant wind.

In section II, the UAV path following problem is described. The path following algorithms for straight line and orbit are introduced in section III, together with simulation results. The comparison between the standard vector field method and the proposed adaptive vector field method is discussed in section IV. Finally, the section V concludes this work.

II. PROBLEM DESCRIPTION

The vector field (VF) method is based on specifying a desired course at a certain coordinate. This method is used for straight line and orbit arcs. More complicated paths can be segmented with straight lines and arcs ([8], [9]).

Some assumptions are listed here to clarify the limitations and study ground of this paper.

Assumption 1: Altitude and airspeed (V_a) are held constant by the longitudinal control of UAV.

Assumption 2: The UAV is equipped with the course-hold loop devices whose dynamics can be modeled as the first-order system

$$\dot{\chi'} = \alpha(\chi_c - \chi')$$

where χ' is the real course of the UAV, i.e. the angle between its ground velocity and the horizontal axis in the earth frame, χ_c is the command course from the controller, and α is a known positive constant that defines the response speed of the course-hold loop.

Assumption 3: The UAV course is measurable.

Assumption 4: The wind field consists of a constant component with magnitude W, angle ψ_w and a slowly time-varying unknown component with amplitude $A(t)$ and angle $\psi_A(t)$.

Remark 1: Assumptions 1, 2 and 3 are standard in most VF strategies ([6], [7], [8], [10], [11]). Assumption 4 relaxes the classical assumption where the wind vector is completely known.

In the numerical studies done in this work, we take the following environmental conditions: the magnitude of the time-varying component is changing over time in a co-sinusoidal fashion with frequency 0.1 rad/sec, the angle of the time-varying component is changing in a sinusoidal fashion with frequency 0.1 rad/sec. All the parameters related to the time-varying component of the wind are unknown to the designer. The designer only knows the constant component of the wind, whose parameters are considered as:
Constant wind's amplitude: $W = 6$;
Constant wind's angle: $\psi_w = 230°$;
Time-varying wind's amplitude: $A(t) = 3\cos(0.1t)$;
Time-varying wind's angle: $\psi_A(t) = \pi\sin(0.1t)$.

Under assumptions 1-4, the relationship between UAV airspeed, ground velocity and wind velocity can be illustrated in Fig. 1, resulting in the following navigational dynamics of the UAV:

$$\begin{aligned}\dot{x} &= V_a\cos\psi + W\cos\psi_w + A\cos\psi_A \\ \dot{y} &= V_a\sin\psi + W\sin\psi_w + A\sin\psi_A\end{aligned} \tag{1}$$

where ψ is the heading angle between airspeed and horizontal axis in earth frame, V_a is UAV airspeed, W and A are the amplitude of constant and time-varying part of wind, ψ_w and ψ_A are the angle between constant or time-varying part of wind velocity and x axis in the earth frame. x and y are the coordinate of the earth frame. The value of W and ψ_w can be obtained from historical data of wind velocity, while $A(t)$ and $\psi_A(t)$ can be regarded as disturbances which are slowly changing over time.

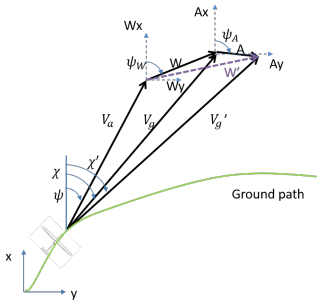

Fig. 1. UAV kinematics and relations between airspeed, ground velocity and wind velocity

From Fig. 1, the UAV velocity in x, y direction can also be expressed by the ground speed and course

$$\begin{aligned}\dot{x} &= V_g'\cos\chi' \\ \dot{y} &= V_g'\sin\chi'\end{aligned} \tag{2}$$

where V_g' is the ground velocity of UAV. Note that V_g' is not measurable since the time-varying wind influences the amplitude of ground velocity.

The overall wind field is denoted with amplitude W' and angle $\psi_{w'}$, which are a combination of constant and time-varying parts

$$\begin{aligned}W'\cos\psi_{w'} &= W\cos\psi_w + A\cos\psi_A \\ W'\sin\psi_{w'} &= W\sin\psi_w + A\sin\psi_A\end{aligned} \tag{3}$$

In the design of vector fields and wind estimators, two fundamental paths are considered: the straight line and orbit paths.

III. Path Following Algorithm

A. Straight Line Following

The objective of straight line following is to steer the UAV to the desired line in the vector field. With respect to [6], a small modification is presented in order to generalize the method for arbitrary lines and arbitrary directions. The error distance e from UAV to desired line in y direction and the desired course χ_d are defined as:

$$\begin{aligned}e &= y - (ax + b) \\ \chi_d &= i\chi^\infty\frac{2}{\pi}\tan^{-1}(ke) + \tan^{-1}(a)\end{aligned}$$

where $ax+b$ defines the line equation of desired path, (x, y) is the coordinate of UAV in the ground reference frame, i defines the direction of UAV movement. When $i = 1$, the UAV goes to the negative direction of x axis. When $i = -1$, the UAV goes to the positive direction of x axis. k is a positive constant which influences the rate of course transition from χ^∞ to steady state course $\tan^{-1}(a)$.

Similar to the Lyapunov stability analysis in [6], Lyapunov function $\mathcal{V}_1 = \frac{1}{2}e^2$ can be used to argue that e will converge to zero if $\chi' \to \chi_d$.

$$\begin{aligned}\dot{\mathcal{V}}_1 &= e(\dot{y} - a\dot{x}) \\ &= eV_g'(\sin\chi_d - a\cos\chi_d) \\ &= eV_g'\frac{\sin(i\chi^\infty\frac{2}{\pi}\tan^{-1}(ke))}{\cos(\tan^{-1}a)}\end{aligned}$$

It is easy to check the $\dot{\mathcal{V}}_1$ is smaller than zero for $e \neq 0$ whatever the e and i are positive or negative. Thus it means that error distance e converges to zero asymptotically if $\chi' \to \chi_d$.

Let $\mathcal{V}_2 = \frac{1}{2}\tilde{\chi}'^2$, where $\tilde{\chi}' = \chi' - \chi_d$ is the error between UAV course and desired course. The derivative of $\mathcal{V}_2$ is

$$\begin{aligned}\dot{\mathcal{V}}_2 &= \tilde{\chi}'\dot{\tilde{\chi}}' \\ &= \tilde{\chi}'(\alpha(\chi_c - \chi') - i\chi^\infty\frac{2}{\pi}\frac{k\dot{e}}{1+(ke)^2}) \\ &= \tilde{\chi}'(\alpha(\chi_c - \chi') - i\chi^\infty\frac{2}{\pi}\frac{k}{1+(ke)^2}V_g'(\sin\chi' - a\cos\chi'))\end{aligned}$$

Ideally, if we choose the command course as:

$$\chi_c = \chi' + \frac{i}{\alpha}\chi^\infty\frac{2}{\pi}\frac{k}{1+(ke)^2}V_g'(\sin\chi' - a\cos\chi') - \frac{\kappa}{\alpha}sat(\frac{\tilde{\chi}'}{\epsilon}) \tag{4}$$

where sat is the saturation function used to eliminate chattering of sign function.

$$sat(x) = \begin{cases}x, & \text{if} \quad |x| < 1 \\ sign(x) & \text{otherwise}\end{cases}$$

and $\kappa > 0, \epsilon > 0$ are the parameters that control the shape of the trajectories on sliding surface and the width of the

transition region around the sliding surface respectively. Then the derivative of $\mathcal{V}_2$ equals

$$\dot{\mathcal{V}}_2 = \begin{cases} -\frac{\kappa}{\epsilon}\tilde{\chi}'^2 & \text{if} \quad |\frac{\tilde{\chi}'}{\epsilon}| < 1 \\ -\kappa|\tilde{\chi}'| & \text{otherwise} \end{cases}$$

which is always negative semi-definite. We conclude that χ' converges to the desired course χ_d in finite time.

However, the control law in (4) cannot be implemented in practice since V_g' is not measurable. In this case, an estimator is designed to estimate the ground velocity of UAV. The control law will be modified as:

$$\chi_c = \chi' + \frac{i}{\alpha}\chi^\infty \frac{2}{\pi}\frac{k}{1+(ke)^2}\hat{V_g}'(\sin\chi' - a\cos\chi') - \frac{\kappa}{\alpha}sat(\frac{\tilde{\chi}'}{\epsilon}) \tag{5}$$

where $\hat{V_g}'$ is the estimated value of V_g'. The following stability result can be stated.

Theorem III.1: In straight line following scenario, the command course (5) and the estimator

$$\dot{\hat{V}}_g' = -\Gamma\rho\tilde{\chi}' i\chi^\infty \frac{2}{\pi}\frac{k}{1+(ke)^2}(\sin\chi' - a\cos\chi') - \sigma\Gamma\hat{V_g}' \tag{6}$$

with $\Gamma > 0$ being the estimation gain and $\sigma > 0$ being a switching σ-modification parameter, guarantees that the tracking error converges to zero for unknown constant winds and stays bounded for unknown slowly time-varying wind.

Proof: For lack of space, the proof is given under the assumption that the derivative of V_g' is negligible. To handle time-varying wind, a σ-modification method [12] must be used: the complete proof will be given in an extended version of this work.

The adaptive law of $\hat{V_g}'$ is derived based on the Lyapunov argument below. Let $\Theta = \hat{V_g}' - V_g'$ be the estimation error. Consider the Lyapunov function $\mathcal{V}_e = \mathcal{V}_1 + \rho\mathcal{V}_2 + \frac{1}{2}\Gamma^{-1}\Theta^2$ whose derivative is

$$\dot{\mathcal{V}}_e = \dot{\mathcal{V}}_1 + \rho\dot{\mathcal{V}}_2 + \Gamma^{-1}\Theta\dot{\Theta}$$

where ρ is the positive weight term for course error in order to make the distance error and course error in the same altitude. Γ is the positive gain for the estimator.

Substitute (5) into the derivative of Lyapunov function $\mathcal{V}_e$

$$\begin{aligned}\dot{\mathcal{V}}_e = \dot{\mathcal{V}}_1 &+ \rho\tilde{\chi}'[i\chi^\infty\frac{2}{\pi}\frac{k}{1+(ke)^2}(\hat{V_g}' - V_g')(\sin\chi' - a\cos\chi') \\ &- \kappa sat(\frac{\tilde{\chi}'}{\epsilon})] + \Gamma^{-1}(\hat{V_g}' - V_g')(\dot{\hat{V}}_g' - \dot{V_g}')\end{aligned}$$

The derivative of the Lyapunov function is

$$\begin{aligned}\dot{\mathcal{V}}_e &\approx \dot{\mathcal{V}}_1 + \rho\tilde{\chi}'[i\chi^\infty\frac{2}{\pi}\frac{k}{1+(ke)^2}(\hat{V_g}' - V_g')(\sin\chi' - a\cos\chi') \\ &\quad - \kappa sat(\frac{\tilde{\chi}'}{\epsilon})] + \Gamma^{-1}(\hat{V_g}' - V_g')\dot{\hat{V}}_g' \\ &= \dot{\mathcal{V}}_1 - \rho\kappa\tilde{\chi}' sat(\frac{\tilde{\chi}'}{\epsilon}) + \{\dot{\hat{V}}_g'\Gamma^{-1} + \rho\tilde{\chi}' i\chi^\infty\frac{2}{\pi}\frac{k}{1+(ke)^2} \\ &\quad (\sin\chi' - a\cos\chi')\}(\hat{V_g}' - V_g')\end{aligned}$$

As we have proved before, $\dot{V}_1$ and $-\rho\kappa\tilde{\chi}' sat(\frac{\tilde{\chi}'}{\epsilon})$ are negative semi-definite. So if the derivative of the estimated ground velocity is chosen as:

$$\dot{\hat{V}}_g' = -\Gamma\rho\tilde{\chi}' i\chi^\infty\frac{2}{\pi}\frac{k}{1+(ke)^2}(\sin\chi' - a\cos\chi') \tag{7}$$

The derivative of V_e will be negative semi-definite.

Next, we use Barbalat's Lemma [13] to prove e and $\tilde{\chi}'$ will converge to zero asymptotically.

$$\begin{aligned}\ddot{\mathcal{V}}_e &= \ddot{\mathcal{V}}_1 - \rho\kappa sat(\frac{\tilde{\chi}'}{\epsilon})\dot{\tilde{\chi}}' \\ &= \ddot{\mathcal{V}}_1 - \rho\kappa sat(\frac{\tilde{\chi}'}{\epsilon})[i\chi^\infty\frac{2}{\pi}\frac{k}{1+(ke)^2}(\sin\chi' - a\cos\chi')\Theta \\ &\quad - \kappa sat(\frac{\tilde{\chi}'}{\epsilon})]\end{aligned} \tag{8}$$

$\tilde{\chi}$, e and Θ are bounded since $\dot{\mathcal{V}}_e \le 0$. It also implies $\ddot{\mathcal{V}}_e$ is bounded based on (8). Hence equivalently $\dot{\mathcal{V}}_e$ is uniformly continuous. Combined with the $\mathcal{V}_e$ is bounded and $\dot{\mathcal{V}}_e$ is negative semi-definite. It infers that $\dot{\mathcal{V}}_e$ converges to zero asymptotically according to Barbalat's Lemma, which also means e and $\tilde{\chi}$ converge to zero asymptotically. ■

In practice, the estimation of ground velocity rate in (6) (or (7)) is modified with a feedforward term which gives the information on how V_g' changes depending on the course.

$$\begin{aligned}\dot{\hat{V}}_g' &= \frac{\partial V_g'}{\partial\chi'}[i\chi^\infty\frac{2}{\pi}\frac{k}{1+(ke)^2}(\sin\chi' - a\cos\chi') - \kappa sat(\frac{\tilde{\chi}'}{\epsilon})] \\ &\quad - \Gamma\rho\tilde{\chi}' i\chi^\infty\frac{2}{\pi}\frac{k}{1+(ke)^2}(\sin\chi' - a\cos\chi') - \sigma\Gamma\hat{V_g}'\end{aligned} \tag{9}$$

where the first term in (9) represents $\dot{V_g}'$. The relationship between ground velocity and course can be derived from (1), (2) and (3) [14].

$$V_g' = W'\cos(\psi_w' - \chi') + \sqrt{V_a^2 - W'^2\sin^2(\psi_w' - \chi')} \tag{10}$$

Since the whole wind field is unknown, W' and ψ_w' are substituted with the constant component of wind W and ψ_w in (10). The partial derivative of ground velocity over course is approximately calculated as

$$\begin{aligned}\frac{\partial V_g'}{\partial\chi'} &\approx \frac{\partial V_g}{\partial\chi'} \\ &= W\sin(\psi_w - \chi') + [V_a^2 - W^2\sin^2(\psi_w - \chi')]^{-\frac{1}{2}}W^2 \\ &\quad \sin(\psi_w - \chi')\cos(\psi_w - \chi')\end{aligned} \tag{11}$$

The whole path following strategy for straight line is illustrated in the control scheme in Fig. 2.

The control scheme is implemented in Simulink, using a desired line described by $y = 0.5x$ in Fig. 3. Four different cases of design parameters (k, κ and ϵ) are compared with each other in Fig. 4. In all simulations, $\sigma = 0$ because this choice delivered good performance and thus it was not necessary to tune this extra parameter.

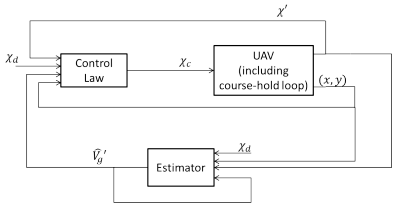

Fig. 2. Scheme of straight line path following

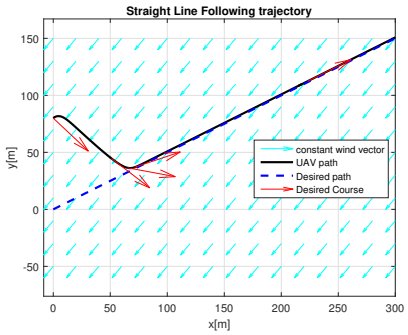

Fig. 3. Straight line following performance

The design parameters affect the transient behavior of UAV in the following manner. Larger k makes the UAV's transient performance faster. Smaller κ makes the transient trajectory smoother and slower. The parameter ϵ can be tuned to avoid chattering.

The steady state performance of straight line following strategy can be evaluated by the root mean square (RMS) tracking error between the desired path and the real UAV position, excluding the transient tracking errors from the turns. The root mean square error of the four cases in Fig. 4 are summarized in Tab. I. Steady state is assumed when the distance from the desired path settles inside the bounds $\pm 0.1m$.

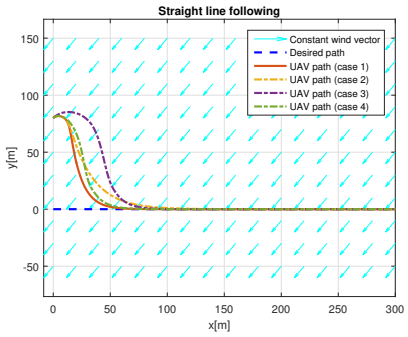

Fig. 4. Influence of design parameters for straight line following:
Case 1: $k = 0.1, \kappa = \frac{\pi}{2}, \epsilon = 0.5, \Gamma = 50$;
Case 2: $k = 0.05, \kappa = \frac{\pi}{2}, \epsilon = 0.5, \Gamma = 50$;
Case 3: $k = 0.1, \kappa = \frac{\pi}{6}, \epsilon = 0.5, \Gamma = 50$;
Case 4: $k = 0.1, \kappa = \frac{\pi}{2}, \epsilon = 1.5, \Gamma = 50$.

The performance of the estimator is evaluated with two criteria including transient RMS estimation error and steady RMS estimation error. In Fig. 5, it can be noted that the estimator does not track the real ground velocity. This could be caused by lack of persistence of excitation. The estimator errors for three different estimator gains are in Tab. II.

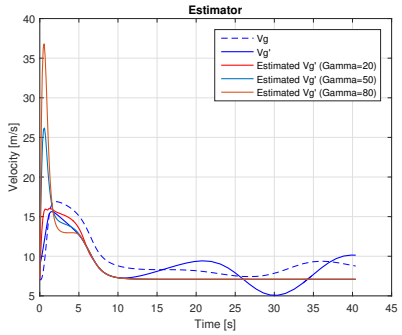

Fig. 5. Estimation performance in straight line following

B. Orbit Path Following

The strategy for orbit path following is similar to the straight line following where the vector field is built up around the desired orbits. The UAV position is expressed in the circular coordinates where the origin locates at the orbit center. The distance from the orbit center to the UAV is denoted with d. And the angular position of UAV is denoted with γ. We assume the orbit center (c_x, c_y) and radius r of the desired orbit are known. The relationship between circular coordinates and Cartesian coordinates is

$$\begin{aligned} x &= c_x + d\cos\gamma \\ y &= c_y + d\sin\gamma \end{aligned} \tag{12}$$

Substitute (12) into (2). The dynamics of UAV is

$$\begin{aligned} \dot{d} &= V_g' \cos(\chi' - \gamma) \\ \dot{\gamma} &= \frac{V_g'}{d} \sin(\chi' - \gamma) \end{aligned}$$

The desired course which steers the UAV towards the desired path was proposed in [6]

$$\chi_d = \gamma + j[\frac{\pi}{2} + \tan^{-1}(k\tilde{d})]$$

where j indicates the direction of desired orbit. When $j = 1$, a counterclockwise orbit is applied. When $j = -1$, a clockwise orbit is applied. $\tilde{d} = d - r$ is the distance error.

TABLE I

TRACKING ERROR FOR 4 DIFFERENT SETS OF DESIGN PARAMETERS

	Case 1	Case 2	Case 3	Case 4
RMS	0.0196	0.0254	0.0185	0.0228

TABLE II

ESTIMATION ERROR FOR 3 ESTIMATOR GAINS

Estimation gain	Transient RMS error	Steady RMS error
$\Gamma = 20$	0.9283	1.6280
$\Gamma = 50$	2.8929	1.6399
$\Gamma = 80$	4.7111	1.5886

Similar to the Lyapunov argument for straight line following, the Lyapunov function $\mathcal{V} = \frac{1}{2}\tilde{d}^2 + \frac{1}{2}\rho\tilde{\chi}'^2$ will be used to derive the command course for the UAV. The derivative of $\mathcal{V}$ is

$$\begin{aligned}\dot{\mathcal{V}} &= \tilde{d}\dot{\tilde{d}} + \rho\tilde{\chi}'\dot{\tilde{\chi}}' \\ &= -V_g'\tilde{d}\sin(\tan^{-1}(k\tilde{d}))+ \\ &\quad \rho\tilde{\chi}'[\alpha(\chi_c - \chi') - \frac{V_g'}{d}\sin(\chi-\gamma) - j\beta V_g'\cos(\chi'-\gamma)]\end{aligned} \tag{13}$$

It is evident that the first term in (13) is always negative. So if the command course is chosen as

$$\chi_c = \chi' + \frac{V_g'}{\alpha d}\sin(\chi-\gamma) + j\frac{\beta}{\alpha}V_g'\cos(\chi'-\gamma) - \frac{\kappa}{\alpha}sat(\frac{\tilde{\chi}'}{\epsilon})$$

$\dot{V}$ will be negative semi-definite, which means that $\tilde{d}, \tilde{\chi}'$ will converge to zero. Since the V_g' is unknown, the control law needs to be modified in a similar manner as the straight line following case. This results in

$$\chi_c = \chi' + \frac{\hat{V}_g{}'}{\alpha d}\sin(\chi-\gamma) + j\frac{\beta}{\alpha}\hat{V}_g{}'\cos(\chi'-\gamma) - \frac{\kappa}{\alpha}sat(\frac{\tilde{\chi}'}{\epsilon}) \tag{14}$$

Theorem III.2: In orbit path following scenario, the command course (14) and the estimator

$$\dot{\hat{V}}_g' = -\Gamma\rho\tilde{\chi}'(\frac{\sin(\chi'-\gamma)}{d} + j\beta\cos(\chi'-\gamma)) - \sigma\Gamma\hat{V}_g{}' \tag{15}$$

with $\Gamma > 0$ being the estimation gain and $\sigma > 0$ being a switching σ-modification parameter, guarantees the tracking error converges to zero for unknown constant winds and stays bounded for unknown slowly time-varying wind.

Proof: The proof follows similar steps as the proof of Theorem III.1 and it is not given for lack of space: the complete proof will be given in an extended version. ■

In practice, a feedforward term representing the variation of the wind can be added to (15). We obtain

$$\begin{aligned}\dot{\hat{V}}_g' &= \frac{\partial V_g'}{\partial\chi'}(\frac{V_g'}{d}\sin(\chi'-\gamma) + j\beta\cos(\chi'-\gamma) - \kappa sat(\frac{\tilde{\chi}'}{\epsilon})) \\ &\quad - \Gamma\rho\tilde{\chi}'(\frac{\sin(\chi'-\gamma)}{d} + j\beta\cos(\chi'-\gamma)) - \sigma\Gamma\hat{V}_g{}'\end{aligned} \tag{16}$$

where the first term in (16) represents $\dot{V}_g{}'$ and $\frac{\partial V_g'}{\partial\chi'}$ is approximated as (11). The whole control scheme of orbit path following is similar to the straight line following scenario. Fig. 6 illustrates the influence of the design parameters on the performance of orbit path following, using four different choices of design parameters. In all simulations, $\sigma = 0$ because this choice delivered good performance and thus it was not necessary to tune this extra parameter. The RMS tracking errors at steady state are summarized in Tab. III. Case 1 behaves better than the other cases. It indicates that larger k is beneficial for the steady state performance at the expenses of transient performance.

In Fig. 7, the estimator performance for the orbit path following works better than the straight line following since it can track the real ground velocity closely (possibly due to the fact that the circular path generates some persistence of excitation). Larger estimator gain will improve the steady estimation of ground velocity at the expense of large overshoot in transient performance, as summarized in Tab. IV.

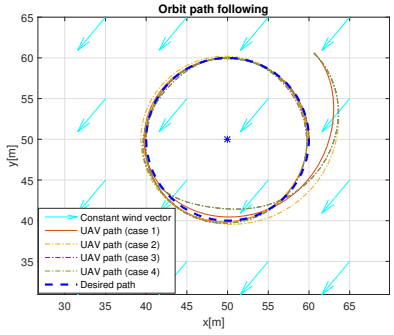

Fig. 6. Influence of design parameters for orbit following:
Case 1: $k = 0.1, \kappa = \frac{\pi}{2}, \epsilon = 0.5, \Gamma = 50$;
Case 2: $k = 0.05, \kappa = \frac{\pi}{2}, \epsilon = 0.5, \Gamma = 50$;
Case 3: $k = 0.1, \kappa = \frac{\pi}{6}, \epsilon = 0.5, \Gamma = 50$;
Case 4: $k = 0.1, \kappa = \frac{\pi}{2}, \epsilon = 1.5, \Gamma = 50$.

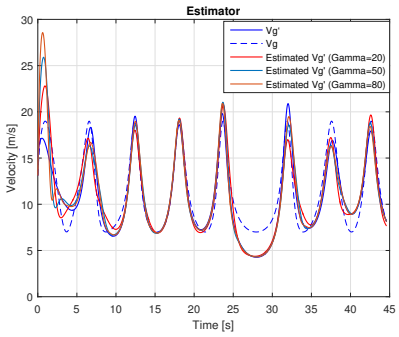

Fig. 7. Estimator performance in orbit path following

TABLE III
TRACKING ERROR FOR 4 DIFFERENT SETS OF DESIGN PARAMETERS

	Case 1	Case 2	Case 3	Case 4
RMS	0.1423	0.2004	0.1921	0.1921

TABLE IV
ESTIMATION ERROR FOR 3 ESTIMATOR GAINS

Estimation gain	Transient RMS error	Steady RMS error
$\Gamma = 20$	2.5419	1.1052
$\Gamma = 50$	3.0363	0.6949
$\Gamma = 80$	3.5641	0.4908

IV. EVALUATION OF THE ALGORITHM

The comparison among three methods for path following is presented here. The three methods are the standard VF method (which assumes to know the constant wind vector only), the ideal VF method (which assumes to know both

the constant wind vector and the time-varying wind vector) and the proposed adaptive VF method.

The root mean square error between the desired path and the real path in steady state is used to evaluate the steady state performance of these three methods. The performance for straight line following is shown in Fig. 8 and Tab. V. For the transient behavior, the proposed method is slightly faster than the others. And the steady state RMS error is smaller than standard VF method. Meanwhile, the performance of orbit path following is shown in Fig. 9 and Tab. VI. It is obvious that the proposed adaptive VF method is superior to the standard VF method in both transient and steady states.

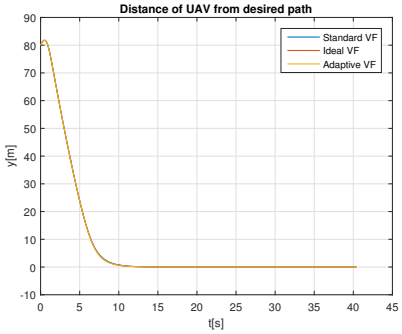

Fig. 8. Distance of UAV from the desired path using 3 different methods

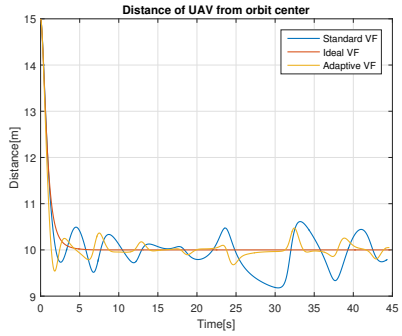

Fig. 9. Distance of UAV from orbit center using 3 different methods

TABLE V

STEADY STATE RMS ERROR FOR STRAIGHT LINE FOLLOWING

Method	Standard VF	Ideal VF	Adaptive VF
RMS	0.2203	0.1573	0.1434

TABLE VI

STEADY STATE RMS ERROR FOR ORBIT FOLLOWING

Method	Standard VF	Ideal VF	Adaptive VF
RMS	0.33	6.08×10^{-6}	0.1219

V. CONCLUSION

This paper presented an adaptive vector field method for the UAV path following under slowly time-varying wind environment. The proposed method was developed for two scenarios: straight line following and orbit following. The combination of Lyapunov stability argument, σ-modification and Barbalat's Lemma are used to analytically prove that the path following errors are bounded under unknown slowly time-varying winds. Numerical simulations have been presented to show the feasibility of the adaptive VF method. The simulations indicate the adaptive VF method has better performance than the standard VF method, especially in the orbit path following scenario. In future works, we would like to address larger uncertainties using adaptive supervisory tools [15] [16]. Furthermore, the adaptive VF method would be implemented on real UAVs and the performance would be tested in practice.

REFERENCES

[1] P. B. Sujit, S. Saripalli, and J. B. Sousa, "Unmanned aerial vehicle path following: A survey and analysis of algorithms for fixed-wing unmanned aerial vehicless," *IEEE Control Systems*, vol. 34, no. 1, pp. 42–59, Feb 2014.

[2] M. Kothari, D. W. Gu, and I. Postlethwaite, "An intelligent suboptimal path planning algorithm using rapidly-exploring random trees," in *Control Conference (ECC), 2009 European*, Aug 2009, pp. 677–682.

[3] A. Ratnoo, P. Sujit, and M. Kothari, "Adaptive optimal path following for high wind flights," *18th IFAC World Congress, Milano*, vol. 44, no. 1, pp. 12 985 – 12 990, 2011.

[4] F. Gavilan, R. Vazquez, and S. Esteban, "Trajectory tracking for fixed-wing uav using model predictive control and adaptive backstepping," *1st IFAC Workshop on Advanced Control and Navigation for Autonomous Aerospace Vehicles ACNAAV15 Seville, Spain*, vol. 48, no. 9, pp. 132 – 137, 2015.

[5] G. Ambrosino, M. Ariola, U. Ciniglio, F. Corraro, E. D. Lellis, and A. Pironti, "Path generation and tracking in 3-d for uavs," *IEEE Transactions on Control Systems Technology*, vol. 17, no. 4, pp. 980–988, July 2009.

[6] D. R. Nelson, D. B. Barber, T. W. McLain, and R. W. Beard, "Vector field path following for miniature air vehicles," *IEEE Transactions on Robotics*, vol. 23, no. 3, pp. 519–529, June 2007.

[7] E. W. Frew, D. A. Lawrence, C. Dixon, J. Elston, and W. J. Pisano, "Lyapunov guidance vector fields for unmanned aircraft applications," in *2007 American Control Conference*, July 2007, pp. 371–376.

[8] H. Chen, K. Chang, and C. S. Agate, "Uav path planning with tangent-plus-lyapunov vector field guidance and obstacle avoidance," *IEEE Transactions on Aerospace and Electronic Systems*, vol. 49, no. 2, pp. 840–856, APRIL 2013.

[9] Y. Liang and Y. Jia, "Combined vector field approach for 2d and 3d arbitrary twice differentiable curved path following with constrained uavs," *Journal of Intelligent & Robotic Systems*, vol. 83, no. 1, pp. 133–160, 2016.

[10] T. A. Johansen, A. Cristofaro, K. Sorensen, J. M. Hansen, and T. I. Fossen, "On estimation of wind velocity, angle-of-attack and sideslip angle of small uavs using standard sensors," *2015 International Conference on Unmanned Aircraft Systems, ICUAS 2015*, pp. 510–519, 2015.

[11] J. D. Barton, "Fundamentals of small unmanned aircraft flight," *Johns Hopkins Apl Technical Digest*, vol. 31, pp. 132–149, 2012.

[12] P. A. Ioannou and S. Baldi, "Robust adaptive control," *In The Control Systems Handbook, Second Edition: Control System Advanced Methods, William S. Levine (Ed.), CRC Press*, pp. 35–1–35–22, 2010.

[13] H. Khalil, *Nonlinear Systems*, ser. Pearson Education. Prentice Hall, 2002.

[14] R. W. Beard and T. W. McLain, *Small unmanned aircraft: Theory and practice*. Princeton University Press, 2012.

[15] S. Baldi and P. A. Ioannou, "Stability margins in adaptive mixing control via a lyapunov-based switching criterion," *IEEE Transactions on Automatic Control*, vol. 61, pp. 1194–1207, 2016.

[16] S. Baldi, G. Battistelli, D. Mari, E. Mosca, and P. Tesi, "Multi-model unfalsified switching control of uncertain multivariable systems," *International Journal of Adaptive Control and Signal Processing*, vol. 26, pp. 705–722, 2012.